Jestr

Journal of Engineering Science and Technology Review 16 (2) (2023) 131 - 137

Research Article

JOURNAL OF
Engineering Science and Technology Review

www.jestr.org

Polar Constrained Image Stitching Algorithm for Unmanned Aerial Vehicle Based on Crossing Area

Ji Ma[1], Wenci Liu[1,*], Linlin Ding[1], Hao Luo[1] and Ye Zhao[2]

[1]College of Information, Liaoning University, Shenyang 110036, China
[2]New World CO.,LTD, Fukuokaken 8300033, Japan

Received 19 January 2023; Accepted 30 April 2023

Abstract

Stitching the aerial images from an Unmanned Aerial Vehicle (UAV) is usually needed to obtain a more comprehensive image information, but the image stitching technology is limited by the requirements of stitching quality and stitching speed. This study proposed a method to achieve good quality, fast stitching speed, and good robustness in image stitching. A large number of feature points in the intersection region were extracted and incorrect feature matching point pairs were accurately filtered out. The area with large cross area of multiple images was extracted as the target area of feature points to be extracted. The Scale-Invariant Feature Transform (SIFT) algorithm was employed to extract the feature points in the image which was not invariant with illumination, environment, and scale. Given that Brute Force (BF) matching soundly produces large number of wrong feature point pairs, the polar constraint was added to improve the matching accuracy, and the feature point pairs were further filtered through the Progressive Sample Consensus (PROSAC) algorithm. Finally, the homograph transformation matrix was used for image registration, and the fusion algorithm was applied to naturally fuse the two images together. Results demonstrate that this algorithm largely reduces the computational complexity, improves the speed by 0.124% compared with other algorithms, and improves the performance of Root Mean Square Error (RMSE) and Mean Square Error (MAE) by 0.224% and 0.173%, respectively. The stitched image quality is obviously better than the general algorithm process. The proposed method provides a certain reference for UAV aerial image Mosaic methods.

Keywords: Image stitching, Cross areas, Polar constraints, PROSAC

1. Introduction

In recent years, Unmanned Aerial Vehicle (UAV) has been widely used in all walks of life. UAV has the characteristics of flexible take-off and landing, low operating costs, and easy operation [1]. Agricultural irrigation, terrain detection, and target tracking are areas where UAV is being used with increasing frequency. The demand for UAV has shown a gradual increase while also seeing remarkable progress in the related technical research with growing units using UAV for image information acquisition. In 2000, the American professor, Shmuel Peleg, used images from aerial photography by UAVs and divided them into narrow strips for multiple projections to complete the stitching of images, opening up a new breakthrough in image stitching in the field of aerial photography by UAVs [2].

However, with the demand for obtaining further information from images, obtaining large-area observation images became difficult for UAV remote sensing [3]. Therefore, stitching the acquired remote-sensing images was necessary to improve the information-gathering capability of remote-sensing images [4]. Owing to the limitations of flight height and camera focal length, images captured by UAV have many undesirable characteristics, such as large numbers, small image ranges, and high levels of overlap. They also require aerial UAV photography to extend the field of view for many specific tasks, which still seems challenging with the current imagery technology.

In the existing research, scholars have also carried out substantial research on the traditional image stitching technology, but certain shortcomings persist in terms of stitching speed and stitching quality [5-10]. For example, image ghosting, distortion, misalignment, and other aspects lead to poor final stitching quality results. Thus, an urgent need arises to solve the problem of how to quickly stitch together a good and smooth panorama.

Based on above analysis, this study proposed a method to extract a large number of feature points in the intersection region and accurately filter out incorrect feature matching point pairs. The results proposed in this study have a marked increase in image matching speed and a substantial improvement in image-matching quality. In turn, the study provides a certain reference for the optimization of image stitching technology.

2. State of the art

Substantial research and improvement are currently being done by scholars in the field of aerial UAV photography. For example, a Grid-based Motion Statistics (GMS)-Random Sample Consensus (RANSAC) based mosaic algorithm for UAV aerial images is used to obtain the correct set of high-quality interior points while reducing the number of iterations of the algorithm; this process decreases the time complexity of the algorithm without the speed of stitching for images where the scale has been transformed [11]. The classical Scale-Invariant Feature Transform (SIFT)

*E-mail address: liuwenci1225@163.com
ISSN: 1791-2377
doi:10.25103/jestr.162.17

algorithm has disadvantages such as high dimensionality of feature descriptors, high computational effort, and low matching efficiency. Therefore, down-sampling of high-resolution images prior to feature detection has been proposed to reduce the number of feature points and improve the efficiency of feature detection. However, a reduction in the number of feature points leads to a reduction in matching accuracy [12]. Lee et al. considered an image stitching algorithm with robustness to large parallax based on the new concept of warping residuals. The main purpose was to alleviate parallax artifacts, but given that it was stitching images with large parallax, it slowed down the stitching [13]. Existing seam stitching algorithms can eliminate ghosting and blurring on the stitched image, whereas distortions and angular distortions caused by image alignment will remain in the stitching results. To address this problem, a stitching strategy based on optimal seams was proposed [14,21]. However, this algorithm also suffers from distortion caused by image alignment or viewpoint distortion.

Scholars have proposed a method of dividing images into dense grids, each corresponding to a chi-square matrix, which highly improves the alignment of the image. At the same time, the workload upfront is considerably increased [15]. This splice layer was searched by defining the grey-scale weighted distance and the differential gradient-domain as the differential split. However, the computational complexity increases [16]. Then, the Speed-Up Robust Features (SURF) algorithm was used to stitch aerial images from UAVs and found it to be faster than the SIFT algorithm at matching images. However, the number of matching points was small and unevenly distributed, and the image stitching quality was low [17]. To change the problem of image distortion, Lin et al. proposed a homologous linearization method that smoothly extrapolates the distortion from overlapping regions to non-overlapping regions. However, this method could lead to the original high number of feature points being pushed into non-overlapping areas, which will ultimately lead to a decrease in the accuracy of the stitching [18]. Eden et al. proposed a two-step optimal seaming algorithm that can smoothly seam images. However, the algorithm suffers from scene motion and alignment errors [19]. Superpixel segmentation of the overlapping regions of the reference image was performed to determine the best stitching position precisely. However, determining images with severe distortion was still difficult [20,22]. The traditional algorithm was proposed by various methods, but the essential distortion and blurring and ghosting problems were still not fully resolved [5-10]. Metadata-based and image-based stitching methods were therefore employed to overcome the challenges of low-altitude, small-scale UAV deployment. However, the situation does not exclude the influence of the external environment, and some uncertainty remains [23].

The above results focus on improving the distortion, ghosting, and image alignment of images, but research scarcely examines matching accuracy and stitching speed. Therefore, the study proposes the extraction of feature points in regions with large crossover areas and the use of the polar line constraint algorithm to improve the accuracy of matching. It is further purified by the Progressive Sample Consensus (PROSAC) algorithm, which has less iteration with faster computation capability than the RANSAC algorithm.

The remainder of the study is organized in the following layout. Section 3 describes the computation of cross regions, the principle of limit constraints, the image stitching process, and the PROSAC algorithm. Section 4 analyzes the superiority and feasibility of the algorithm proposed in this study in concrete terms through experiments. Section 5 summarizes the conclusions.

3. Methodology

3.1 Cross-area detection

Owing to external environmental interference, such as foggy days, rain, wind, and other elements, maintaining a consistent UAV flight speed, flight direction, and flight posture while using a UAV for aerial photography might be challenging. These situations caused images to look blurry, distorted, compressed, and magnified. Thus, the result of fine image stitching has a certain effect. These studies indicate that the feature points will be discovered in the region with large cross areas in many images because it is one of the crucial phases in image stitching to identify the feature points of the image.

3.1.1 Calculation of cross areas

The prerequisite for extracting the intersection area of aerial images of UAVs is to know the distance of the UAV from the ground. Therefore, we first have to calculate the flight altitude of the UAV and the calculation formula is as follows:

$$\mathrm{a} = \frac{GSD * f}{c} \tag{1}$$

where GSD is the ground resolution, which refers to the minimum distance between two targets on the captured image. f is the focal length of the camera, and c is the pixel size of the camera. When the camera and its pixels are determined on board the UAV, f and c are also determined. From the above formula, it can be seen that the higher the altitude of the UAV, the lower the ground resolution, i.e., the lower the clarity and accuracy of the image. When the UAV flies at a low altitude, let the height and width of the image ground coverage area H and W, the camera angle of view β; from the above formula, we can know the flight altitude of the UAV a; then, the image resolution, where h and w are expressed as the vertical and horizontal pixel values of the image, respectively, can be derived according to the trigonometric function.

$$W = \frac{2a\tan(\beta/2)}{h^2 + w^2} \tag{2}$$

$$H = \frac{Wh}{\mathrm{w}} \tag{3}$$

The following illustrates three instances of typical UAV aerial photography overlapped areas. To locate the UAV's coordinates, we use Global Positioning System (GPS) signals. Once we have this information, we can use the formula above to calculate the size of the intersection area and set a threshold. Only overlapping ratios that are higher than the threshold of the image pair to match are considered. The target area for feature point identification may then be utilized to be the portion of the region with the largest intersection area.

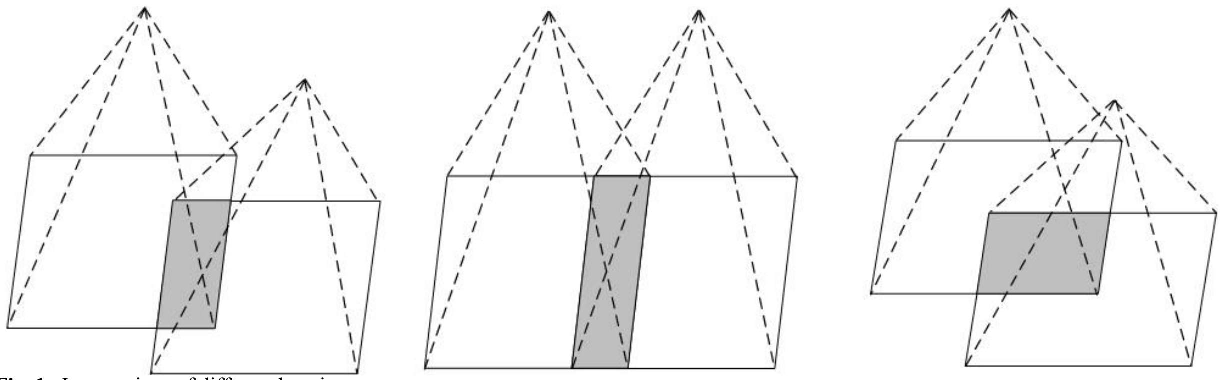

Fig. 1. Intersections of different locations

As UAVs photograph different terrains and may not fly at the same altitude, the above equation creates difficulty in measuring the area measured by the UAV when it is flying at a high altitude. Therefore, this study also proposes a solution to this situation using the semi-positive vector formula to calculate the distance between two points on the surface of a region. With two points X and Y, γ_x and ς_x denoted as the longitude and latitude of X, respectively, the following distances between points X and Y can be obtained from the GPS coordinates.

$$d(X,Y) = 2R\tan[\sin^2(\frac{\gamma_y - \gamma_x}{2}) + \cos(\gamma_x)\cos(\gamma_y)\sin^2(\frac{\varsigma_y - \varsigma_x}{2})]^{\frac{1}{2}} \quad (4)$$

In the equation above, R is the radius of the Earth and the angle between the X and Y points, and the center of the Earth is the azimuth.

$$\theta(X,Y)=\tan^{-1}[2(\frac{\sin(\gamma_y - \gamma_x)\cos(\varsigma_y)}{\cos(\varsigma_x)\sin(\varsigma_y)-\sin(\varsigma_x)\cos(\varsigma_y)\cos(\gamma_y-\gamma_x)}] \quad (5)$$

The distance and azimuth are computed using the GPS coordinates of each imaging center, and the UAV camera route is then created accordingly. The total coverage area is then determined. To identify the feature points, the intersection of many images with a significant rate of overlapping is located.

3.2 Polar constraint

The Brute Force (BF) solution algorithm actually creates a brute force matcher. First, it randomly selects a feature point in the first image. Then, it performs the distance measurement with all the feature points in the second image. Finally, it returns the closest feature point, and the matching result can be obtained. The BF solution algorithm is a rough calculation. The calculation amount is not only large but will also obtain several wrong feature matching pairs. Consequently, this study adds a polar constraint method. The polar constraint is actually a point-to-line constraint and not a point-to-point constraint. Nonetheless, this process allows the polar constraint to give the constraint condition of the corresponding point, which compresses the corresponding point matching from the whole image to identify the corresponding point on a straight line. The latter narrows the search area, which is an effective way to improve matching efficiency and reduce matching errors.

3.2.1 How polar constraints work

When two cameras capture scenes in the same area, a geometric correspondence occurs between the camera and the system composed of the captured scene. As shown in the Fig. 2, O_1 and O_2 represent the centers of the two cameras, P is a point in three-dimensional space, and PO_1O_2 is a polar plane. The junction of O_1 and O_2 becomes the baseline, and the intersection points of the polar plane and the imaging plane are l_1 and l_2, respectively. The intersection points of the baseline and the imaging plane are e_1 and e_2, respectively. As the P point changes in space, the polar plane rotates around the axis of the pole.

For two images I_a and I_b taken in the same scene, any point on I_a will have a corresponding pole line on I_b, and the point in I_b that matches that point must also be on that pole. Therefore, erroneous pairs of matching points can be filtered out by polar constraints. In Fig. 2, three-dimensional vectors X and Y contain correlation points, and the limit constraint equation can be represented by the following formula:

$$Y^T FX = 0 \quad (6)$$

The base matrix is an algebraic description of the polar geometric relationship between two viewpoint images taken by a general perspective camera. The base matrix is a singular 3rd order singular matrix with seven degrees of freedom and the following properties:

$$Fe_1 = 0$$
$$Fe_2 = 0 \quad (7)$$

Fig. 4 also shows that all pixels on the pole line where the same polar plane intersects on the left correspond to the same polar line on the right, forming a correspondence in units of polar lines. If you can find all the corresponding polar pairs, then, matching becomes convenient. Binocular stereo vision by polar line correction is used to complete this step.

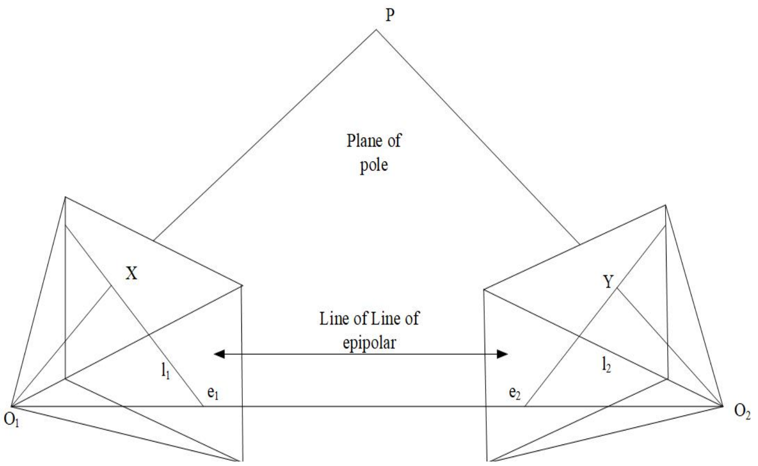

Fig. 2. Corresponding geometric diagram

Through calibrated camera parameters, the image is projected onto a plane parallel to the baseline so that the main optical axes of the two cameras are parallel to each other. Through this setup, the intersection of the polar plane and the two images is in the same scan line. In this way, the same polar pair is in the same row of two images, i.e., the x-coordinate of the feature point pair must be the same, but the y-coordinate may not be. Thus, the polar constraint step is added as a coarse match in the image stitching process.

3.4 Stitching process

The algorithm process of UAV aerial image stitching based on the polar constraint of the intersection area is as follows:

(1) Extract the same intersection area of multiple images.
(2) Use the SIFT algorithm to extract features and maintain the maximum point of the response value.
(3) Apply the BF matching algorithm, add the pole line constraints, and filter the false matching point pairs.
(4) Use the PROSAC algorithm to remove the mismatched feature point pairs.
(5) By transforming the matrix,calculate the corresponding parameters.
(6) Use the fusion algorithm to make the image stitching more natural and smoother.

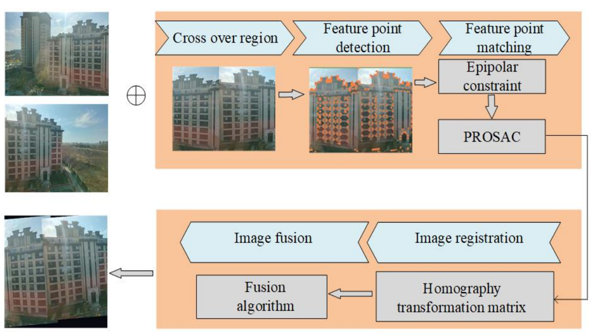

Fig. 3. Block diagram of image mosaic algorithm

3.4 Filter feature matching point pairs

The RANSAC algorithm is frequently used to weed out mismatched feature pairs during the precise matching step, but the RANSAC algorithm's performance has to be increased. The RANSAC method employs random data processing. Therefore, if the percentage of false matches is too large, the algorithm's complexity is enhanced by increasing the number of repetitions. The PROSAC approach, which enhances resilience and computational efficiency and is more appropriate for UAV image stitching, is used in this study. Samples are pre-ordered by mass linearly via PROSAC. Samples that are more similar to one another are more likely to have internal feature points. Next, using the data subset, these internal feature points are retrieved, eliminating blind extraction and considerably enhancing efficiency.

This work enhances the matching algorithm to further raise the PROSAC method's matching accuracy. Second, the matching point pairs are limited by the polar line and organized in decreasing order of Euclidean distance. The permutation is used to obtain the first reliable data. The samples from this collection are then collected and examined. The loop ends if the inner point's value exceeds the predetermined value. Unless the stop condition is satisfied, the value is raised, and the preceding process is repeated.

4 Result Analysis and Discussion

4.1 Evaluation indicators

The algorithm evaluation metrics in this study include four aspects: correct matching rate, execution time, Root Mean Square Error (RMSE), and Mean Square Error (MAE).

(1) Correct match rate: N_t indicates the number of correct matches and N_m indicates the total number of matches. The more the number of correct matchings, the higher the correct rate of matching, the better the quality of stitching.

$$C_{MR} = \frac{N_t}{N_m} \times 100\% \tag{8}$$

(2) Execution time: the shorter the execution time, the more efficient the stitched image will be.

(3) RMSE: RMSE is the root mean square error, M and N denote the length and width of the image, respectively. $f^{`}(i,j)$ and $f(i,j)$ denote the coordinates of the image to be evaluated and the coordinates of the original image, respectively.

$$RMSE = \sqrt{\frac{1}{N}\sum_{i=1}^{N}[f(i,j) - f^{'}(i,j)]^{2}} \tag{9}$$

(4) MAE: MAE is the mean absolute error, which represents the average of the absolute errors between the predicted and observed values.

$$MAE = \frac{1}{N}\sum_{i=1}^{N} | f(i,j) - f^{'}(i,j) | \tag{10}$$

4.2 Polar line image effect display

By experimenting with different algorithms, the figure below shows the matching of feature points. As seen from the Fig. 4, the SURF algorithm feature matching is disorganized with many wrong matching point pairs, which is not ideal. From the figure below, we can see that the Oriented Fast and Rotated Brief (ORB) algorithm detects fewer feature points, which is insufficient to support the later alignment steps. Accelerated-KAZE(AKAZE) algorithm has some feature points that are not successfully matched, and some are incorrectly matched with poor results. Therefore, this study adopts the polar line constraint to match the feature point pairs, thereby improving the matching speed and reducing the computational effort. As can be seen from the Fig. 2, the feature points based on the polar line constraint method in Section 3.2 are all on a straight line and uniquely determine a point corresponding to it. Considering that the polar line constraint also has parallax, the polar line constraint serves as the first coarse matching and filters out most of the wrong matching point pairs. However, the achieved effect remains very obvious and better than the general feature matching.

4.3 Splicing effect and evaluation index shown under different scenes

Based on the methodological theory in Section 3, the final results are demonstrated.

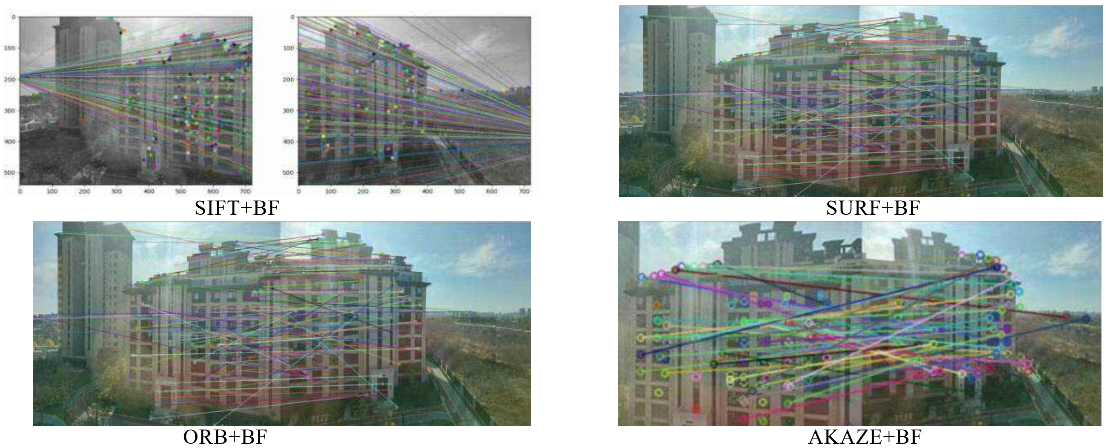

Fig. 4. Comparison before and after adding the limit constraint

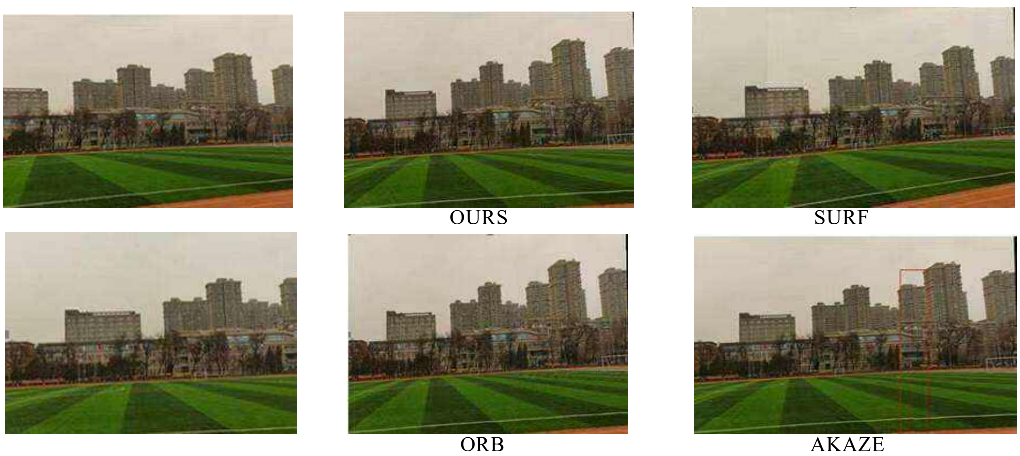

Fig.5. The first set of effects is shown

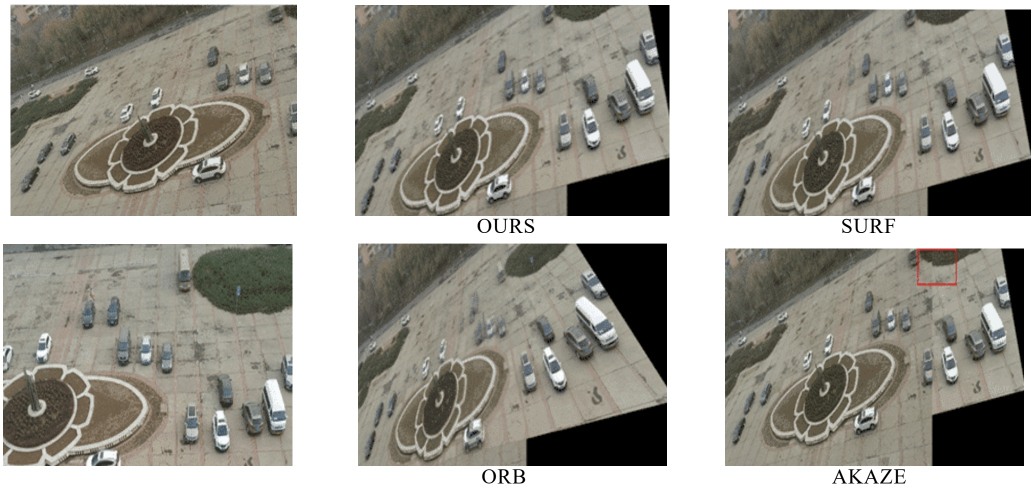

Fig.6. The second set of effects is shown

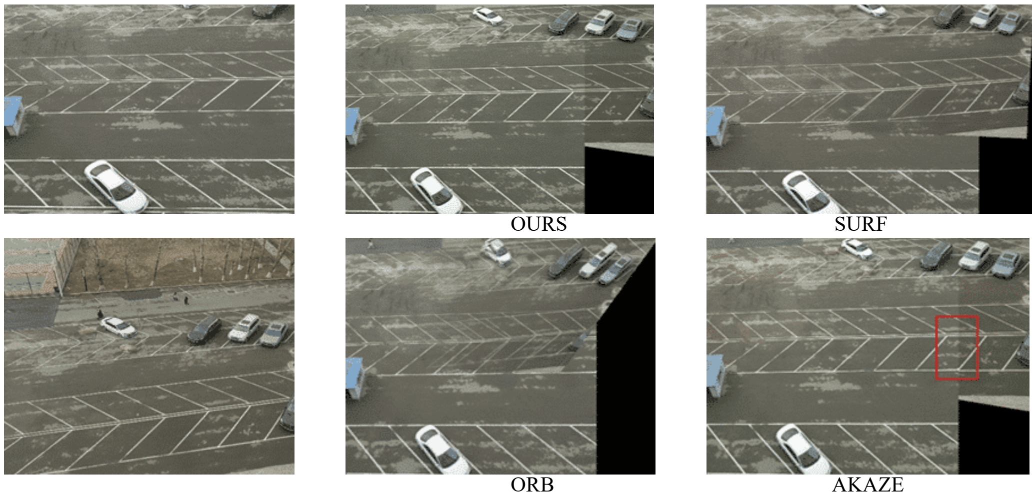

Fig.7. The third set of effects is shown

From the Fig. 5, we can see that under the hazy weather condition, the overall stitching of the SURF algorithm looks flat, but the effect of alignment and de-shadowing is still not good enough. The image stitched by the ORB algorithm looks blurred, the image stitched by the AKAZE algorithm has only some lines left unaligned, and the overall stitching effect remains good. Compared with these three algorithms, this study uses the algorithm stitched image; no blur or alignment inaccuracy exists, the whole picture looks smooth and flat, and stitching quality is better.

The above images show the second set of effects is shown. The SURF algorithm stitched the image with slight ghosting and only stitched a small number of scenes. The ORB algorithm stitched results can show that the ghosting phenomenon is serious, resulting in blurred images, and the AKAZE algorithm only stitched a small part of the scenes as shown in the red box in the Fig 6. Finally, this study shows most of the scenes with no ghosting, no distortion, and stable performance. The following table shows the evaluation indexes of the algorithm. The results show that the algorithm in this study is significantly better than the other algorithms in terms of stitching time and performance.

The third group of scenes shows obvious line segments. The SURF algorithm has ghosting, and the line segments are not aligned. The ORB algorithm stitches the image with serious distortion and ghosting. The AKAZE algorithm has a smooth image surface, and the line segments are not aligned at the red box. The algorithm in this study is precisely aligned, and the image is clear and smooth. The evaluation indexes in the following table also show the superiority of the algorithm.

Table 1. First group of image mosaic effect evaluation

Method	Evaluation Indicators			
	C_{MR} (%)	Execution Time(/s)	RMSE	MAE
OURS	**97.22**	0.041	**0.4167**	**0.3562**
SURF	95.74	0.662	0.5844	0.4573
ORB	93.88	0.674	0.6645	0.5644
AKAZE	96.35	**0.039**	0.4265	0.4289

Table 2. Second group of image mosaic effect evaluation

Method	Evaluation Indicators			
	C_{MR} (%)	Execution Time(/s)	RMSE	MAE
OURS	**98.32**	**0.010**	**0.3998**	**0.3244**
SURF	96.34	0.285	0.5774	0.4216
ORB	94.68	0293	0.6254	0.5239
AKAZE	97.66	0.029	0.4033	0.4278

Table 3. Third group of image mosaic effect evaluation

Method	Evaluation Indicators			
	C_{MR} (%)	Execution Time(/s)	RMSE	MAE
OURS	**97.57**	**0.029**	**0.4211**	**0.3458**
SURF	96.44	0.049	0.5645	0.4318

ORB	95.98	0.050	0.5667	0.5123
AKAZE	96.64	0.048	0.5449	0.4276

It can be seen from Table 1, Table 2 and Table 3 that the algorithm in this paper is nearly 0.124% ahead of other algorithms in matching time, and the RMSE and MAE are also significantly better than other algorithms. In general, the algorithm in this paper has better performance.

5. Conclusions

To create fast, good quality, and robust UAV aerial images stitching, the intersection region of the image was extracted as the target region for feature point detection based on the polar line constraint algorithm, thus determining the unique feature matching point in the two photos. The correct rate of feature point pairs was further improved by the PROSAC algorithm. The following conclusions could be drawn:

(1) A large number of feature points could be extracted in the region with a large intersection area, and the number of matched pairs increases significantly.

(2) The polar line constraint algorithm was used to identify a unique matching point pair in two images.

(3) The PROSAC algorithm was used to further purify the feature-matching point pairs while reducing the computational effort and largely improving the alignment accuracy.

This study combines theory and experiment to propose a new method that will deal with the problem in the process of image stitching technology. The proposed stitching method can be applied to a variety of fields, such as remote sensing positioning, agricultural monitoring, and terrain surveying. In the future, further processing speed can be attempted to generate stitched images of UAV images or videos in real time.

Acknowledgements

This work was supported by the Basic Scientific Research Project of Liaoning Provincial Department of Education (LJKFZ20220174), the National Natural Science Foundation of China (No.62072220,61502215), the Central Government Guides Local Science and Technology Development Foundation Project of Liaoning Province (No.2022JH6/100100032), the Natural Science Foundation of Liaoning Province (2022-KF-13-06), China.

References

1. Liu, C., Zhang, S. and Akbar, A. "Ground Feature Oriented Path Planning for Unmanned Aerial Vehicle Mapping". *IEEE Journal of Selected Topics in Applied Earth Observations and Remote Sensing*, 12(4), 2019, pp.1175-1187.
2. Shmuel, P., Benny, R., Alex, Rav-Acha. "Mosaicking on Adaptive Manifolds". *IEEE Transactions on Pattern and Machine Intelligence*, 22(10), 2000, pp.1144-1154.
3. Li, X., Feng, R., Guan, X., Shen, H., Zhang, L. "Remote sensing image mosaicking: Achievements and challenges". *IEEE Geosocial, Remote Sens*, Mag, 7, 2019, pp.8-22.
4. Jiang, X., Ma, J., Jiang, J. and Guo, X. "Robust Feature Matching Using Spatial Clustering with Heavy Outliers". *IEEE Transactions on Image Processing*, 29, 2000, pp.736-746.
5. Li, Y., Hongmei,Q., Huawen,S. "Research on security risk assessment of SCADA system based on the cloud model and combination weighting". *CAAI Transactions on Intelligent Systems*, 17(5).2022, pp. 969-979.
6. Cui, H., Li, Y. and Zhang, K. "A Fast UAV Aerial Image Mosaic Method Based on Improved KAZE". *2019 Chinese Automation Congress (CAC)*, 2019, pp.2427-2432.
7. Min, H., Kuo, Y., Qin, S. "Image Mosaic algorithm for UAV Aerial Photography based on improved KAZE". *Anti-Counterfeiting Trade Agreement Automatic Sinical*, 45(02), 2019, pp.305-314.
8. Haichang, Z., Yinping, M. "Uav Aerial Image Mosaic Algorithm based on Improved ORB". *Industrial Control Computer*, 31(05), 2018, pp.90-92.
9. Yuanting, X., Yi, L., Kun, Y. and Chunxue, S. "Research on image mosaic of low altitude UAV based on Harris corner detection". In: *2019 14th IEEE International Conference on Electronic Measurement & Instruments*, Changsha, China: IEEE, 2019, pp.639-645.
10. Yang, L., Zhong, J.H., Zhang, Y., Bai, S.C., Li, G.S., Yang, Y. and Zhang, J. "An Improving Faster-RCNN With Multi-Attention ResNet for Small Target Detection in Intelligent Autonomous Transport With 6G". *IEEE Transactions on Intelligent Transportation Systems*, 2022, doi: 10.1109/TITS.2022.3193909.
11. Lan, X., Guo, B., Huang, Z. and Zhang, S. "An Improved UAV Aerial Image Mosaic Algorithm Based on GMS-PROSAC". In:*2020 IEEE 5th International Conference on Signal and Image Processing*, Nanjing, China: IEEE, 2020, pp.148-152.
12. Liu, Y., He, M., Wang, Y., Sun, Y. and Gao, X. "Farmland Aerial Images Fast-Stitching Method and Application Based on Improved SIFT Algorithm". *IEEE Access*, 10, 2022, pp.95411-95424.
13. Lee, K. Y. and Sim, J. Y. "Warping Residual Based Image Stitching for Large Parallax". In:*2020 IEEE/CVF Conference on Computer Vision and Pattern Recognition*, Seattle, WA, USA: IEEE, 2020, pp.8195-8203.
14. Chen, J., Li, Z., Peng, C., Wang, Y., Gong, W. "UAV Image Stitching Based on Optimal Seam and Half-Projective Warp". *Remote Sens*, 14, 2022, pp.1068.
15. Zaragoza, J., Chin, T. J., Brown, M. S., Suter, D. "As-projective-as-possible image stitching with moving DLT". In: *Proceedings of the IEEE Conference on Computer Vision and Pattern Recognition*, Portland, OR, USA: IEEE, 2013, pp.2339-2346.
16. Hejazi, F. H., Khotan, Lou. H. "Fast and robust seam estimation to seamless image stitching". *Signal, Image and Video Processing* , 12,2018, pp.885-893.
17. Hu, T. X., Niu, X. F., Tan, Y. and Chen, X. P. "UAV remote sensing image stitching technology based on surf algorithm". *Mapping Bull*, 60(10), 2015, pp.55-58.
18. Lin, C. C., Pan Kanti, S. U., Ramamurthy, K. N. and Aravkin, A. Y. "Adaptive as-natural-as-possible image stitching". In: *2015 IEEE Conference on Computer Vision and Pattern Recognition*, Boston, MA, USA: IEEE, 2015, pp.1155-1163.
19. Eden, A., Uyttendaele, M., Szeliski, R. "Seamless image stitching of scenes with large motions and exposure differences". In: *Proceedings of the 2006 IEEE Computer Society Conference on Computer Vision and Pattern Recognition*, New York, NY, USA: IEEE,2006, pp.2498-2505.
20. Yuan, Y., Fang, F. and Zhang, G. "Super Pixel-Based Seamless Image Stitching for UAV Images". *IEEE Transactions on Geoscience and Remote Sensing*, 59(2), 2021, pp.1565-1576.
21. Kerschner, M. "Seamline detection in colour orthoimage mosaicking by use of twin snakes". *Journal of Photogrammetry and Remote Sensing*, 56(1), 2001, pp.53-64.
22. Achanta, R., Shaji, A., Smith, K., Lucchi, A., Fua, P., and Süsstrunk, S. "SLIC super pixels compared to state-of-the-art superpixel methods". *IEEE Transactions on Pattern Analysis & Machine Intelligence,* 34(11), 2012, pp.2274-2282.
23. Yahyanejad, S., Wischounig-Strucl, D., Quaritsch, M. and Rinner, B. "Incremental Mosaicking of Images from Autonomous". In:*2010 7th IEEE International Conference on Advanced Video and Signal Based Surveillance*, Boston, MA, USA: IEEE,2010, pp.329-336.